

Design and analysis of a recoil-type vibrotactile transducer

Hsin-Yun Yao

Tactile Labs, Saint-Bruno, Québec, Canada

Vincent Hayward^{a)}

Institut des Systèmes Intelligents et de Robotique, UPMC, Université Paris 06, CC 173-4 Place Jussieu, 75005 Paris, France

(Received 9 February 2010; revised 4 June 2010; accepted 8 June 2010)

This article describes the design of a high-bandwidth, iron-less, recoil-based electromagnetic vibrotactile actuator. Its working principle, the theoretical analysis, the method used to determine its transfer function, its scaling properties and its design constraints are discussed along with its fabrication and possible improvements.

© 2010 Acoustical Society of America. [DOI: 10.1121/1.3458852]

PACS number(s): 43.38.Dv, 43.66.Wv, 43.80.Jz, 43.38.Ar [AJZ]

Pages: 619–627

I. INTRODUCTION

Modern portable communication devices are noted for their ever-increasing data processing and display capabilities. With mixed success, they strive to tap into several human sensory channels: vision, audition and touch. Comparatively, the use of the haptic channel—where movement and touch sensations are combined—in order to exchange information is achieved today only at a very basic level, as discussed in recent surveys.^{1,2}

The only tactile feedback signal widely used in consumer applications is the vibrotactile signal communicated to the user by inducing persistent or transient oscillations to the enclosure or to the front plate of a hand-held device. During operation, these surfaces are normally in contact with the fingers of the user, which makes this approach very practical. If the device is in a pocket, then the large surface of the enclosure makes it possible to radiate sufficient vibration energy for signaling an alert through layers of clothes or even when placed in a handbag. Understandably, this type of signal is easy to create and can elicit salient sensations in exchange of very little electrical power and given a tiny space and cost budget.

A different vibrotactile stimulation approach is employed by the ‘tactor’. A tactor device is designed to stimulate a small region of skin tissue, and often operates like an acoustic transducer. While the tactor has more than eighty years of history since R. H. Gault noticed that the vibration of the membrane of a telephone earpiece caused strong cutaneous sensations,^{3,4} it has not been adopted by the consumer industry. This lack of adoption is likely to be due to the necessity to maintain direct contact between the radiating element and the skin through the use of a strap or of a garment. With the tactor, the regions of stimulation are also restricted to areas that are free of manipulative or sensing purposes, excluding, for instance, the fingertips and the thenar region which are crucial during interaction with a device.

Enclosure or front plate vibration, on the other hand, is almost universally used in portable phones and other devices because it is practical. Oscillations are almost always obtained using vibration motors because they are very efficient in power and space and are easy to commission. Their efficiency arises from their mode of operation which is to spin an eccentric mass attached to the shaft of a dc motor. Their expressive capabilities are—by principle—restricted, as further discussed in the next section. Despite its limitations, it is possible to use vibration motors in direct contact with the skin, making a “one note” tactor out of a vibration motor.⁵

In this paper, we describe a third approach that relies, like the vibration motor, on the production of vibrations in a whole device or plate, but which is capable, like the voice-coil tactor or the loudspeaker, of producing precisely controlled vibrations over a wide frequency bandwidth and dynamic range. This device operates from a recoil principle by establishing a Laplace force between an elastically guided slug—a permanent magnet—and an casing that contains two coils in an open magnetic circuit arrangement.

This new device can be integrated in hand-held enclosures since, unlike voice-coil-driven tactors, it does not require a mechanical ground to operate and, unlike the vibration motor, has all the features of a transducer capable of linear operation over a large range. From a tactile display perspective, an analogy can be drawn with visual displays. Black-and-white binary displays are quite useful, say to display numbers, but many find color images more visually appealing. They also offer new opportunities for interaction designers. The transducer described in this article achieves just that: interaction designers have total freedom over the transmitted vibration waveform.

After a brief background discussion we describe the transducer’s working principle and its model in terms of an equivalent electrical circuit. We then describe a system identification procedure where each component of the circuit is either measured or derived theoretically. The model is then employed to analyze the sensitivity of the complete system performance with respect to each component characteristic. Possible improvements based on this analysis are suggested.

^{a)}Author to whom correspondence should be addressed. Electronic mail: vincent.hayward@isir.upmc.fr

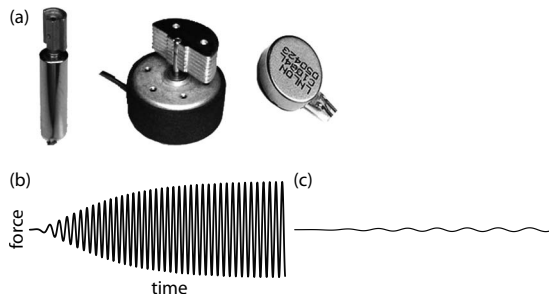


FIG. 1. Vibration Motors and their typical response. (a) Various models from Precision Microdrives Ltd. (b) Chirp-like response of a vibration motor to a step input. (c) Reducing the input amplitude by a factor five renders the motor essentially useless.

II. BACKGROUND

A. Basic vibration motor

For purposes of comparison, let us first describe briefly the mode of operation of vibration motors. Referring to Fig. 1(a), a common design is when an eccentric mass attached to shaft of a small dc motor. Sometimes, the design is integrated as in the model shown in the right-most example of Fig. 1(a).⁶

Consider the limit case when such motor is attached to a rigid mechanical ground. When the motor spins, the interaction force with the ground depends on the square of the angular velocity. The vibration motors used in consumer products typically target an angular velocity in the range of 100–200 rotations per second.⁷ This method makes it possible to vibrate heavy loads provided that dissipative effects do not dominate the small power of the motor. Given a voltage step input of magnitude h , the spinning velocity follows a first order response, $\omega(t) \propto h[1 - \exp(-t/\tau)]$, because the vibrator obeys the general dynamic behavior of a DC motor where the time constant, τ , depends on the ratio of its inertia to its back-EMF coefficient (if the electrical time constant is ignored). The produced centrifugal force is of the form $|f| \propto \omega^2$. If the vibrator is mounted on a case which is much heavier than the spinning mass, then the vibration obeys $h^2[1 - \exp(-t/\tau)]^2 \exp\{jh[1 - \exp(-t/\tau)]t\}$, where the vibration amplitude (the first factor) and the frequency (the exponent) are linked. If we plot the response of a typical vibration motor powered at full amplitude, we obtain a profile such as that seen in Fig. 1(b), where the ramp-up period is in the range of hundreds of milli-seconds. This ramp-up period causes significant delay and is problematic when a precise sensory outcome is desired. As a result, these motors are not suitable for scientific experiments where the temporal properties of the stimulus are important.

To better appreciate the fact that there is little room given to interaction designers to obtain a richer behavior from such motors, Fig. 1(c) shows the response of the same motor when the input step is five times smaller. Not only is the vibration of very low frequency, but its amplitude is also very low. As a result, designers have considered adding additional dynamics to this kind of vibrators,⁸ or have developed more sophisticated control schemes.⁹ Nevertheless, the scope of these improvements is limited.

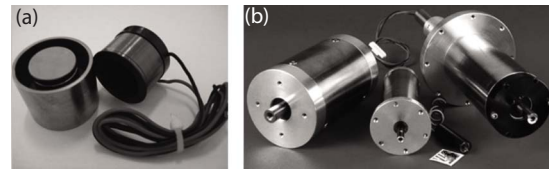


FIG. 2. (Color online) Voice Coil Actuators. Sources: (a) Moving Coil (USA Motion), (b) Moving Magnet (H2W Technologies).

B. Moving-coil and moving-magnet actuators

Moving-coil actuators [one model is represented in Fig. 2(a)], use the same principles as electromagnetic loudspeakers. They comprise a voice coil, a magnet creating an annular field, and a suspension mechanism. Below saturation, the output force is by-and-large linearly determined by the input current. They can be very accurate and do not have bandwidth limitations other than their structural dynamics and the ability of the driving amplifier to push current in an inductive load.

Compared to vibration motors, they are more expensive and generally larger, unless designed to operate at one single resonant frequency. In the latter case, their response magnitude is very sensitive to the presence of any dissipative term in the load which is very detrimental to their role as a transducer. For haptic applications, moving-coil actuators are not very suitable. Often designed to move very small masses, they cannot produce large movements at low frequencies, let alone be imbedded in a portable device.

Some models are designed to operated with a fixed coil and a moving magnet, which can result in a larger output force for a same volume since a fixed coil can be thermally connected to an external heat sink [one model is represented in Fig. 2(b)]. The downside is a larger moving mass and often a more limited displacement range. Moving magnet actuators have been used in research projects for different purposes with different sizes and configurations. At a larger scale, permanent magnet linear actuators are widely used in air compressors.^{10,11} At a small scale, it can be produced with sub-millimeter sizes to use as precision actuator.^{12,13} Because of its simplicity and efficiency, it has a wide spread industrial and research application. Experimental and analytical modeling, optimization, improvements has been extensively discussed in the past.^{14–16}

C. Other prime mover techniques

For vibrotactile haptic applications, other actuating principles have been explored: piezoelectric benders,¹⁷ stacks,¹⁸ and magnetostriction. None of these approaches have approached the potentially low manufacturing cost and the practicality of electromagnetic transducers with either moving magnets or moving coils.

D. Design criteria for recoil-type vibrotactile actuators

The general design criteria of recoil-type vibrotactile actuators are similar to the criteria that apply to many other types of actuators: small size, high specific power, efficiency, ability to be packaged, robustness, linearity, and ease of commissioning. However, they do have some specific con-

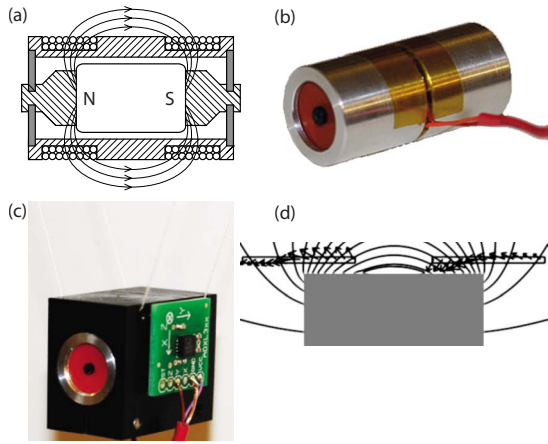


FIG. 3. (Color online) Actuator arrangement. (a) Shaded parts are made of non-ferromagnetic material. A magnet is suspended by two rubber membranes in gray. The field lines intersect each half of the coil to create an axial force. The coil is arranged such that the current flows in opposite directions in each half. (b) External aspect of a 13×25 mm ‘haptuator’. (c) Measurement setup with purely inertial load. (d) The magnetic field lines emanating from the magnet. The arrows show the forces acting on the coil.

straints. Ideally, vibrotactile actuators should be able to provide stimulation from a few Hz to 500 Hz. With recoil-type actuators, providing output the upper frequency range is not difficult, but providing output in the low-end is constrained by a basic tradeoff driven by the scale at which the device is built. For a given output, a reduction of the moving mass must be compensated by a larger peak-to-peak excursion, complicating the suspension design. This is similar to loudspeakers when the area of the membrane is reduced. Informal experiments have shown that 3 G of acceleration is the greatest stimulation at the fingertips that can be sustained before the onset of numbness. This figure was therefore targeted in the present design.

III. ACTUATOR DESCRIPTION

A. Physical description

The actuator, henceforth named an ‘‘haptuator,’’ is an ungrounded moving magnet voice-coil type linear actuator with a moving magnet. Referring to Fig. 3, a cylindrical magnet is suspended by two rubber membranes (in gray) via two non-ferromagnetic pins (hashed lines) inside a tubular enclosure (hashed lines) such that the generated magnetic field intersects the two halves of a coil at mostly right angle. When the current flows through the coil, it interacts with the magnetic field of the permanent magnet to create a Laplace force in the axial direction. The magnet moves axially as a result of this force relatively to the enclosure. The displacement is a function of the Laplace force, of dynamic inertial forces acting on both the enclosure and the magnet, plus elastic and viscous forces developing between the magnet and the enclosure.

Recoil-type actuators can be small. The authors have made extensive use of a version that is 13 mm in diameter, 25 mm in length, see Fig. 3(b), and yet is able to produce several G’s of acceleration given 5 W of input power. Similar designs have been used in a number of previous studies.^{7,19–21} Typically, the actuator was embedded in other

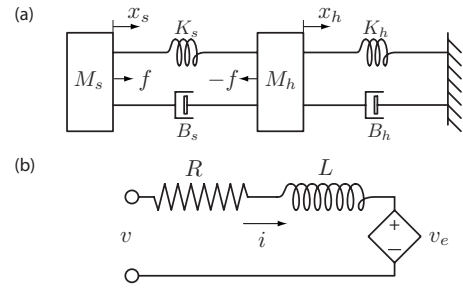


FIG. 4. Actuator physics. (a) Free-body diagram of the actuator. The two masses are free-floating. The ‘s’ parameters can be set by design. The ‘h’ parameters represent the load which must be driven. (b) Electrical circuit.

enclosures or in the handles or larger devices. In these designs, it was easy to arrange for the coil to have a 5 Ω impedance so the actuator could be powered with ordinary audio components.

B. Dynamic model

Denote by $B(l)$, the magnetic flux density created by the permanent magnet where the current i flows in the coil at location l , the Laplace force f is obtained from

$$f = i \oint dl \times B(l) = \gamma i, \quad (1)$$

where γ represents the actuator’s drive factor, or Bl factor. This force, like in a loudspeaker, develops between the coil and the magnet. Since the actuator is intended to operate ungrounded, connected to driven device, its mechanical behavior can be represented by a six-parameter model, see Fig. 4(a).

An electromechanical force is applied to masse M_h , representing the equivalent inertia of the coil assembly, the device enclosure and the apparent hand mass, and to a second mass, M_s , representing the inertia of the slug/magnet. These elements are connected by spring-damper systems, where K_h , B_h represents the load and K_s , B_s represents the suspension. The positions of the masses are denoted x_s and x_h , respectively.

Electrically, the system can be represented by the circuit shown in Fig. 4(b) where, v is the voltage at the terminals, i , the current, v_e , the voltage resulting from Lenz’ law with actuator constant ϵ , R and L , the resistance and inductance of the coil respectively.

From these diagrams, the system’s governing equations can be written as follows,

$$f = M_s \frac{d^2 x_s}{dt} + B_s \frac{d(x_s - x_h)}{dt} + K_s(x_s - x_h), \quad (2)$$

$$-f = M_h \frac{d^2 x_h}{dt} + B_h \frac{dx_h}{dt} + K_h x_h$$

$$-B_s \frac{d(x_s - x_h)}{dt} - K_s(x_s - x_h), \quad (3)$$

$$f = \gamma i, \quad (4)$$

TABLE I. Electrical equivalents to mechanical elements using the impedance or the mobility analogy.

Mechanical	Impedance	Mobility
Force f	Voltage $v: f \rightarrow v$	Current $i: f \rightarrow i$
Velocity \dot{x}	Current $i: \dot{x} \rightarrow i$	Voltage $v: \dot{x} \rightarrow v$
Mass M	Inductor $L: M \rightarrow L$	Capacitor $C: M \rightarrow C$
Spring K	Capacitor $C: K \rightarrow 1/C$	Inductor $L: K \rightarrow 1/L$
Damper B	Resistor $R: B \rightarrow R$	Resistor $R: B \rightarrow 1/R$

$$v_e = \epsilon \frac{d(x_s - x_h)}{dt}, \quad (5)$$

$$v = Ri + L \frac{di}{dt} - v_e. \quad (6)$$

C. Equivalent circuit

A practical approach to analyze mechatronic systems is to convert the mechanical part into an electrical equivalent circuit. Once connected to an electrical driver circuit, the complete system can then be analyzed in the time or in the frequency domain although it may be made of components governed by mechanical, electrical, hydraulic, or acoustical laws. Once these interconnected components are converted into a single circuit, the contributions of each element can be studied using circuit theory. Such an approach has been extensively used to analyze acoustic transducers and enclosures,²²⁻²⁴ and it is the method adopted in this article.

To find the equivalent circuit of a mechanical system, one can proceed with either the impedance or the mobility analogy. The two analyses are equivalent, and the choice is often based on the form of the governing laws in each domain.²⁵ After replacing the mechanical elements into its electrical equivalent using the conversion Table I, each element can be connected in a way that satisfies the conservation laws. For example, using the mobility analogy, if two mechanical elements are subject to the same force, their electrical counterparts must be connected in series to share the same current; if they are forced to move at the same velocity, their counterparts must be connected in parallel in order to drop the same voltage. It must be nevertheless remembered that these analogies are mere tools for analysis and often lead to interpretations that do not possess a valid physical significance.²⁵

From the mechanical free-body diagram, one obtains two equations describing the different forces acting on M_s and M_h ,

$$0 = M_s \frac{d\dot{x}_s}{dt} + B_s(\dot{x}_s - \dot{x}_h) + K_s \int (\dot{x}_s - \dot{x}_h) - f, \quad (7)$$

$$0 = M_h \frac{d\dot{x}_h}{dt} + B_s(\dot{x}_h - \dot{x}_s) + K_s \int (\dot{x}_h - \dot{x}_s) + f + B_h \dot{x}_h + K_h \int \dot{x}_h. \quad (8)$$

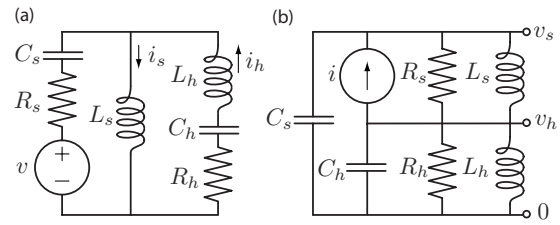


FIG. 5. Equivalent circuit. (a) Using the impedance analogy. (b) Using the mobility analogy.

When employing the impedance analogy an inductor L is a substitute for a mass M , the inverse of a capacitance, $1/C$, for a stiffness, K , a resistance, R , for a damper, B , a current, i , for a velocity, \dot{x} , such that equations that describes force balances become voltage loop equations,

$$0 = L_s \frac{di_s}{dt} + R_s(i_s - i_h) + \frac{1}{C_s} \int (i_s - i_h) - v, \quad (9)$$

$$0 = L_h \frac{di_h}{dt} + R_s(i_h - i_s) + \frac{1}{C_s} \int (i_h - i_s) + v + R_h i_h + \frac{1}{C_h} \int i_h, \quad (10)$$

$$0 = L_s \frac{di_s}{dt} + L_h \frac{di_h}{dt} + R_h i_h + \frac{1}{C_h} \int i_h. \quad (11)$$

To obtain the electric circuit described by the these equations, one considers them as the application of Kirchhoff's voltage law for two loops in a circuit. The current in each branch is such that the three loops form a circuit shown in Fig. 5(a).

Similarly, to use the mobility analogy, C is a substitute for M , $1/L$ for K , $1/R$ for B , voltage v for velocity \dot{x} , such that the equations that describe force equilibria become current summations at the nodes as shown in Fig. 5(b),

$$0 = C_s \frac{dv_s}{dt} + \frac{v_s - v_h}{R_s} + \frac{1}{L_s} \int (v_s - v_h) - i, \quad (12)$$

$$0 = C_h \frac{dv_h}{dt} + \frac{v_h - v_s}{R_s} + \frac{1}{L_s} \int (v_h - v_s) + i + \frac{v_h}{R_h} + \frac{1}{L_h} \int v_h, \quad (13)$$

$$0 = C_s \frac{dv_s}{dt} + C_h \frac{dv_h}{dt} + \frac{v_h}{R_h} + \frac{1}{L_h} \int v_h. \quad (14)$$

The above equations can be viewed as the result of the application of Kirchhoff's current laws to three nodes of a circuit, where the current flowing through each element is equal to the voltage at its terminals divided by its impedance.

Figure 6 shows the equivalent circuits of the mechanical system using the impedance and mobility analogies [panel (a) and (b) respectively]. These transformations result in circuits that are dual to each other, and solving one is equivalent to solving the other. Note that for the impedance analogy, the values of the impedances are the inverse of the

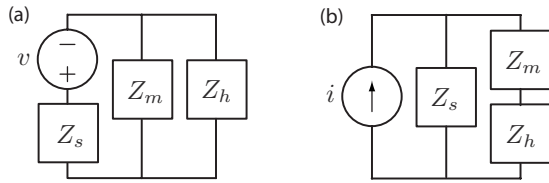


FIG. 6. Block representation of the mechanical components, (a) impedance, (b) mobility.

values for the mobility analogy ($Z \rightarrow 1/Z$) because of their duality properties. Despite the inverse relationship, all have the unit of Ohm (Ω).

One important advantage of translating a mechanical system into an equivalent electrical circuit is that it can be combined with the electrical driver circuitry, and the whole mechatronic system can be analyzed in a unified manner. Specifically, because audio amplification components are typically voltage amplifiers, it is more convenient to employ the mobility analogy. (If current amplifiers were used, we would prefer the impedance analogy.) Using the mobility analogy, one may combine the circuits from mechanical and electrical components by means of an ideal transformer of ratio $\gamma : 1$ to represent the force developed between the magnet and the coil, as described by (1) and as shown in Fig. 7(a). The relationship from the input voltage to the output velocity can therefore be determined directly. A similar approach is used in the analysis of loudspeakers driven by voltage amplifiers.

One last transformation can be applied to the system representation to facilitate its analysis. Figure 7(b) shows a circuit equivalent to that of Fig. 7(a) without the ideal transformer, by reflecting the primary side into the secondary side. Solving for the circuit variables now allows us to establish the relationship between the input v and other variables of interest, such as \dot{x}_h .

These transformations can be summarized by expressions in the Laplace domain:

$$Z_c = sL + R, \quad (15)$$

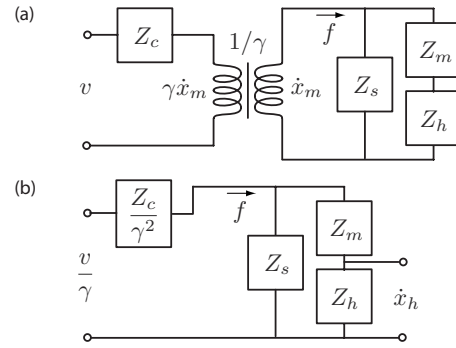


FIG. 7. Circuit representation of the electrical circuit combined with the equivalent circuit of the mechanical system.

$$Z_m = \frac{1}{sC_m} = \frac{1}{sM_m}, \quad (16)$$

$$Z_s = \left(\frac{1}{sL_s} + \frac{1}{R_s} \right)^{-1} = \left(\frac{K_s}{s} + B_s \right)^{-1}, \quad (17)$$

$$Z_h = \left(sC_h + \frac{1}{sL_h} + \frac{1}{R_h} \right)^{-1} = \left(sM_h + \frac{K_h}{s} + B_h \right)^{-1}. \quad (18)$$

IV. SYSTEM IDENTIFICATION

Some parameters such as the mass of the magnet or of the shell, m_m and m_h , as well as input voltage can readily be known or measured. Some others, such as the mechanical impedance of the suspension Z_s , the coil impedance Z_c , and the actuator constant γ require experimental identification.

A. System response and modeling

In a first step the input-output system response was measured when the load was just an inertia, that is, when $K_h=0$ and $B_h=0$. To achieve this condition, we secured the haptuator in a box and suspended it with thin threads. An accelerometer (ADXL320 from Analog Devices) was at-

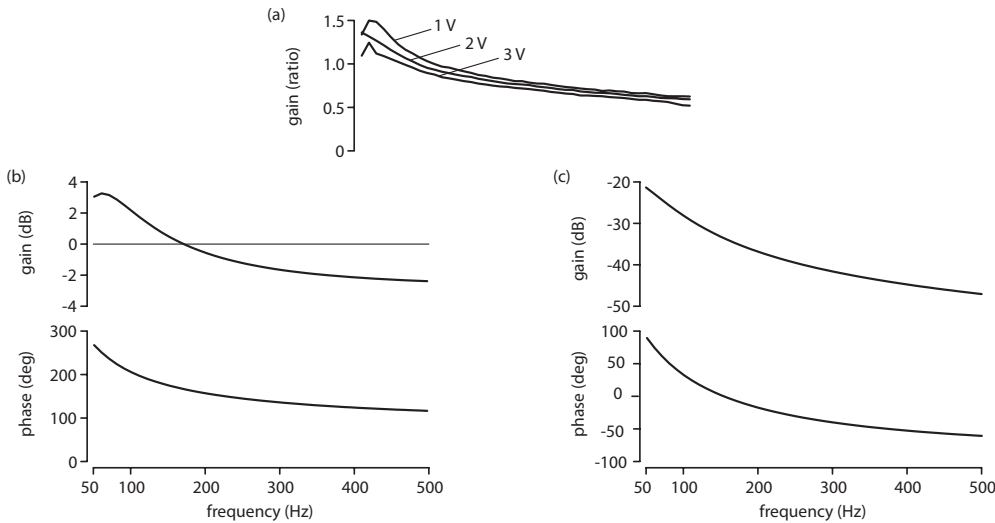


FIG. 8. System Response. (a) Frequency response of the actuator acceleration to input voltage ratio for three different levels (rms). (b) The magnitude and phase plot of a fitted 2nd order model. (c) Plot of the impedance of the suspension, Z_s .

tached to the wall of the box. When activated, the actuator could vibrate freely in the direction parallel to the floor, see Fig. 3(c).

The acceleration response for three different input voltages can be seen in Fig. 8(a). The three responses for 1, 2 and 3 V inputs (rms) do not fall exactly in top of each other (by less than 1 dB). This slight discrepancy is easily explained by saturation effects which are mostly noticeable around the natural resonance. They arise, like for loudspeakers, because the large excursion of the moving part causes the suspension to cease acting linearly, presumably because of the nonlinear characteristics of rubber at high strains, and because the magnetic flux interfering with the coils is no longer constant. In other words, the actuator starts “bottoming out” at resonance for a 3 V input. For this input, the acceleration is by-and-large 3 G throughout the frequency range. For a 1 V input (1 G output for this load), the actuator operates mostly linearly.

The shape of the response resembles that of a 2nd order system with a 60 Hz natural resonance, which decays following one slope up to around 150 Hz, and following another from 150 Hz to 500 Hz, indicating the presence of zeros in the transfer function. A 2nd order model with two poles and two zeros gave an excellent fit ($r^2=0.98$). It is written

$$\hat{H}(s) = \frac{\ddot{x}_h}{v} = \frac{0.685s(s - 1150)}{s^2 + 565.9s + 1.283e5},$$

$$= \frac{as(s - b)}{s^2 + 2\zeta\omega_0s + \omega_0^2}. \quad (19)$$

where the damping coefficient is $\zeta=0.79$ and the resonance frequency $F_0=\omega_0/2\pi=57$ Hz. It is not seen on the figure, but the model gradually differs from the measured response for frequencies above 400 Hz, indicating the possibility of one or several zeros at higher frequencies. These zeros are likely to be due to the accelerometer transfer function (rated bandwidth 500 Hz), but not to the actuator.

B. Parameters found directly

Due to the small number of turns, the inductance of the coil L (found to be 2.05×10^{-8} H) could be neglected in the

frequency range considered, hence Z_c could be measured directly to be $Z_c=5.0 \Omega$. Other parameters directly measurable are the mass of the magnet, $M_m=7$ g, and the mass of the case and of the test box, $M_h=15$ g.

The actuator drive factor, γ , (or ‘ Bl ’ factor) was obtained using two methods: force measurement and simulation.

The first method involved measuring directly the force produced by a DC current. The rubber suspension was removed, and a peg was used to keep the magnet centered. The actuator was placed vertically above a scale such that when a DC current was sent to the coil, the magnet produced a force acting against the scale. Having the force and the current, using Eq. (1), γ can be obtained.

The second method employed a commercial finite element analysis tool (COMSOL 3.5, COMSOL AB, Stockholm, Sweden). The geometry of the actuator was supplied to the simulation, as well as the B field of the magnet, measured to be 0.50 ± 0.01 T at the pole, and the total coil length. The software simulation tool used the above parameters to estimate γ . A plot of the magnetic field lines and the resulting Lorentz force from the simulation can be seen in Fig. 3(d).

Twelve measurements were made with $i=70-143$ mA, using the first method. The factor γ was found to be 0.98 ± 0.06 T·m. The second method gave $\gamma = 0.96 \pm 0.01$ T·m. These values are within each other’s uncertainty range. In the following sections, the mean value of $\gamma=0.97$ T·m is used.

C. Suspension impedance

From Fig. 7(a) the transfer function from voltage to output velocity in terms of the system parameters is

$$\frac{\dot{x}_h}{v} = \frac{\gamma Z_s Z_h}{\gamma^2 Z_s Z_m + Z_c(Z_m + Z_h + Z_s)},$$

$$H(s) = \frac{s \gamma Z_s Z_h}{\gamma^2 Z_s Z_m + Z_c(Z_m + Z_h + Z_s)}. \quad (20)$$

The quantities Z_s , Z_c , Z_m , and Z_h can be substituted in (20) for their expressions, (15)–(18), to give

$$H(s) = \frac{s \gamma Z_s Z_h}{\gamma^2 Z_s Z_m + Z_c(Z_m + Z_h + Z_s)} = \frac{s \gamma (K_s/s + B_s)^{-1} (s M_h)^{-1}}{\gamma^2 (K_s/s + B_s)^{-1} (s M_m)^{-1} + R((s M_m)^{-1} + (s M_h)^{-1} + (K_s/s + B_s)^{-1})}$$

$$= \frac{s^2 \gamma M_m}{s^2 R M_m M_h + s(\gamma^2 M_h + R M_h B_s + R M_m B_s) + R M_h K_s + R M_m K_s}. \quad (21)$$

The transfer function (21) is of 2nd order with two zeros and two poles with two unknown parameters, K_s and B_s that describe a 1st-order suspension model as in (17). Substituting in (20) the values $M_m=0.007$, $M_h=0.015$, $\gamma=0.97$, and $R=5.0$, the transfer function becomes

$$H(s) = \frac{s \gamma Z_s M_m}{Z_s \gamma^2 M_h + R M_h + R M_m + s R Z_s M_m M_h}$$

$$= \frac{64.7s Z_s}{134Z_s + 1.05e3 + 5.0sZ_s}. \quad (22)$$

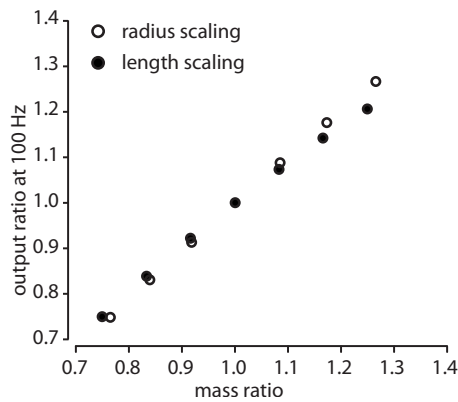


FIG. 9. Actuator scaling properties.

An expression for \hat{Z}_s can be found by relating (22) with the transfer function (19) obtained experimentally,

$$\hat{Z}_s(s) = \frac{11.7(s - 1150)}{s^2 + 659s + 1.37e05} \quad (23)$$

Instead of a 1st-order expression, $Z(s) = (K_s/s + B_s)^{-1}$ from (17), we find a more complicated 2nd-order expression. This can easily be explained by considering that the disk suspension operates as a vibrating membrane. Its actual dynamics are likely to involve high-frequency vibrations modes which were picked up by the experimental identification procedure in the frequency range of interest.

The denominator of (22) suggests that the first term, $134Z_s$, is the dominant term for position of the poles. When comparing the response of Z_s in (23) [see plot in Fig. 8(c)] to the model (19), it is noticed that they share the same zeros at 0 and 1150 rad/s, and that they have poles that are very close to each other (358 vs. 370 rad/s). The resemblance of the transfer function with the suspension impedance suggests that the transfer function is primarily determined by the characteristics of the suspension and shaped by the other parameters.

V. ACTUATOR ANALYSIS

With the help of the parametrized transfer function (20), we can now investigate the impact of each individual parameter on the overall outcome. The effect of each element in (20) is analyzed, except the magnet mass Z_m . The magnet plays a dominant role in the dimensioning of the actuator, and changing it would mean modifying the whole geometry of the actuator. For this reason, the magnet mass Z_m is taken to be the scale parameter.

Figure 9 shows the effect of scaling by varying either the radius or the length of the cylindrical magnet. All other parameters are kept constant, except γ , which was re-evaluated for each case. The figure shows an almost linear relationship between the relative mass of the magnet and the magnitude of the output ratio at 100 Hz. The shape of the frequency response for all cases is almost identical (not shown). There is a slight advantage at scaling radius rather than length. This may be due to the fact that a magnet with a larger radius provides a greater surface for the field lines and therefore gives a larger flux at the location of the coils.

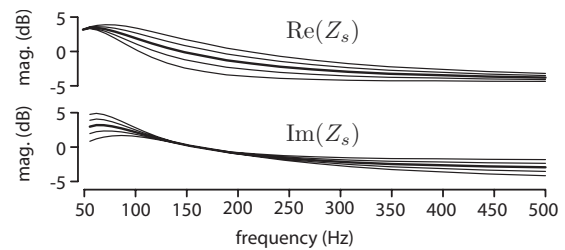


FIG. 10. The magnitude of $H(s)$ when the real (top) and the imaginary part (bottom) of Z_s vary by 20% around the nominal value.

A. Impedance of the suspension: Z_s

As noted in the previous section, Z_s dominates the placement of the system zeros and poles. Physically, the suspension of the actuator is a thin rubber disk designed to be much more compliant in the axial direction than in the radial direction. At high frequencies it behaves like a membrane with vibration modes that gave Z_s a 2nd-order transfer function characteristic (23).

The modification of the material and of the thickness of the suspension would change the acceleration response of the actuator according to (22). Figure 10 shows the variation of $H(s)$ when the real (top) and imaginary (bottom) parts of Z_s vary by $\pm 20\%$ around the nominal value. Varying the real part of Z_s does not have the same effect as varying the imaginary part but both variations shift the resonance and modify its Q-factor.

B. Load inertia Z_h

The primary function of this actuator is to provide a source of vibration. Figure 11(a) shows how different inertia affect the acceleration output, based on (20). As might be

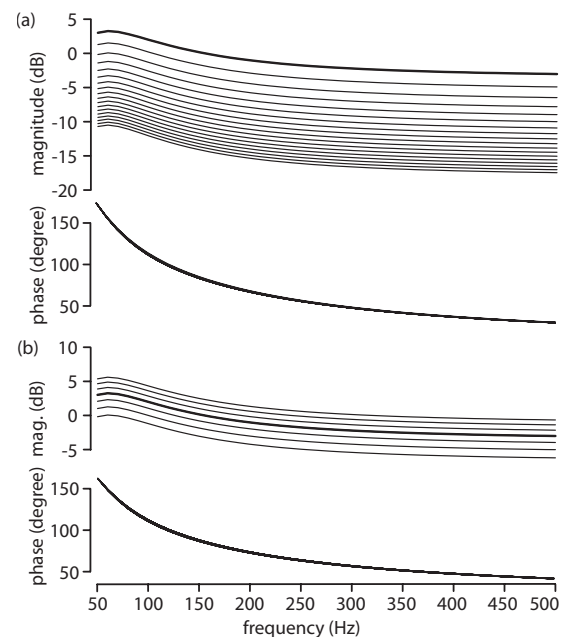


FIG. 11. (a) Acceleration output when the load varies from 15 g to 100 g (lowest) with 5 g increments. The thick line in the magnitude plot with the nominal value of 15 g. (b) Acceleration output for values of γ 30% higher to 30% lower. Each line represents a 10% increment. The thick line in the magnitude plot with the original value, $\gamma=0.97$.

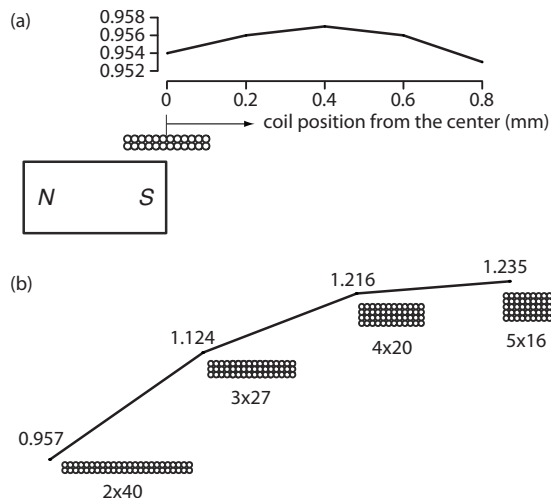


FIG. 12. Coil optimization. (a) Values of γ for different coil positions away from the center position. (b) Actuator drive factor γ given by different coil configuration.

expected, the acceleration output decreases with a larger load. The phase plot, however, is unaffected when Z_h varies from 15 to 100 g in 5 g increments. The higher the mass, the denser the lines, which means that the magnitude doesn't decrease linearly with the increasing mass. The higher the mass, the smaller is the incremental effect on the output deceleration.

C. Actuator drive factor γ

The larger is the B field, the larger is γ . Figure 11(b) shows how a higher value of γ enhances the response. Similarly to Z_h or Z_c , the output magnitude is almost directly proportional to the increase of γ , while the phase behavior remains unchanged. The software analysis tool was also used to investigate different strategies to increase γ without changing significantly the geometry, the size or the electrical characteristics of the haptuator.

1. Coil placement

The coil of the actuator should be placed where the magnetic field is the strongest, which is when the mid-point of the coil is near with edge of the magnet with a small offset, see Fig. 12(a). Because the magnetic field is not completely symmetrical, moving the coil slightly toward the denser area increases the output force. The optimal placement is when the mid-point of the coil is offset by about 0.4 mm with respect to the edge of the magnet.

2. Coil configuration

Another possible optimization is to attempt pack as many turns as possible where the magnetic field is strongest. This can be achieved by shortening the coil length and increasing the number of layers, while keeping the same total number of turns. A tradeoff exists since the field decays radially. Simulations demonstrated that γ improves with the number of layers until the coil thickness becomes large enough to prevent any further improvement, see Fig. 12(b). A thicker coil is also heavier.

TABLE II. Summary of the main characteristic figures.

Parameter	Value
Dimensions (diameter \times length)	14 \times 29 mm
Total mass	23 g
Mass of moving magnet	7 g
Drive factor	0.98 T·m
Acceleration 3 V input, 125 Hz	3.0 G (29.4 m/s ²)
Rated bandwidth	50–500 Hz
Typical impedance	6.0 Ω
Maximum input voltage	3.0 V
Maximum input current	0.5 A

D. Summary of performance figures

The basic design described in this paper is likely to benefit from further optimizations and improvements. Table II summarizes the basic performance figures of the present prototype for future reference.

VI. CONCLUSION

The goal of this paper was to describe, model, and analyze a new type of iron-less recoil actuator. Once a mathematical model of the actuator was obtained, the contribution of each individual components could then be studied separately. We started from a mechanical free-body diagram and then translated it into a equivalent of electrical circuits so that it could be combined with the electrical driving circuitry. We then found the complete system transfer function. While most parameters entering in the coefficients of the transfer function could be measured directly, the suspension and the actuator drive factor γ were identified experimentally. It was verified that γ could be accurately predicted by simulation with finite element analysis tool. By substituting the experimental data into the theoretical equation, it is then possible to find the remaining unknown suspension model.

We then analyzed the sensitivity of each parameter on the overall response. We found that the suspension characteristics impacts the general shape of the response as well as the resonance frequency. In that the haptuator is similar to a loudspeaker. The other components have a direct, linear scaling effect on performance. Increasing γ increases the output proportionally. Moreover, as can be expected, output acceleration decreases with the loads. The actuator also exhibits a simple scaling law. A finite element analysis tool was shown to be able to predict the behavior of the actuator accurately and thus can be used to reliably optimize the overall coil/magnet geometry. Possible improvements were also discussed.

ACKNOWLEDGMENTS

This work was funded in part by the Natural Sciences and Engineering Council of Canada in the form of a Discovery Grant to VH.

¹K. E. MacLean, *Haptic Interaction Design for Everyday Interfaces* (Human Factors and Ergonomics Society, Santa Monica, CA, 2008), pp. 149–194.

²L. A. Jones and N. B. Sarter, "Tactile displays: Guidance for their design

and application," *Hum. Factors* **50**, 90–111 (2008).

- ³R. H. Gault, "Tactual interpretation of speech," *Sci. Mon.* **22**, 126–131 (1926).
- ⁴B. J. Mortimer, G. A. Zets, and R. W. Cholewiak, "Vibrotactile transduction and transducers," *J. Acoust. Soc. Am.* **121**, 2970–2977 (2007).
- ⁵L. A. Jones and D. A. Held, "Characterization of factors used in vibrotactile displays," *J. Comput. Inf. Sci. Eng.* **8**, 044501 (2008).
- ⁶S.-U. Chung, G.-Y. Hwang, S.-M. Hwang, B.-S. Kang, and H.-G. Kim, "Development of brushless and sensorless vibration motor used for mobile phone," *IEEE Trans. Magn.* **38**, 3000–3002 (2002).
- ⁷H.-Y. Yao, D. Grant, and M. Cruz-Hernandez, "Perceived vibration strength in mobile devices: The effect of weight and frequency," *IEEE Transaction on Haptics* **3**, 56–62 (2010).
- ⁸D. Bailey, D. Grant, A. Jasso, E. Shahoin, K. Tierling, and S. Vassallo, "Haptic feedback using rotary harmonic moving mass," U.S. Patent No. 7,161,580 (2007).
- ⁹V. Hayward and K. E. MacLean, "Do it yourself haptics, Part-I," *IEEE Rob. Autom. Mag.* **14**, 88–104 (2007).
- ¹⁰R. E. Clark, G. W. Jewell, and D. Howe, "Dynamic modeling of tubular moving-magnet linear actuators," *J. Appl. Phys.* **93**, 8787–8789 (2003).
- ¹¹L. N. Tutelea, M. C. Kim, M. Topor, J. Lee, and I. Boldea, "Linear permanent magnet oscillatory machine: Comprehensive modeling for transients with validation by experiments," *IEEE Trans. Ind. Electron.* **55**, 492–500 (2008).
- ¹²D. de Bhailís, C. Murray, M. Duffy, J. Alderman, G. Kelly, and S. C. Ó. Mathúna, "Modelling and analysis of a magnetic microactuator," *Sens. Actuators, A* **81**, 285–289 (2000).
- ¹³D. Niarchos, "Magnetic MEMS: Key issues and some applications," *Sens. Actuators, A* **109**, 166–173 (2003).
- ¹⁴N. Bianchi, S. Bolognani, D. D. Corte, and F. Tonel, "Tubular linear permanent magnet motors: An overall comparison," *IEEE Trans. Ind. Appl.* **39**, 466–475 (2003).
- ¹⁵J. Wang, D. Howe, and G. Jewell, "Analysis and design optimization of an improved axially magnetized tubular permanent-magnet machine," *IEEE Trans. Energy Convers.* **19**, 289–295 (2004).
- ¹⁶S. M. Jang, J. Y. Choi, S. H. Lee, H. W. Cho, and W. B. Jang, "Analysis and experimental verification of moving-magnet linear actuator with cylindrical Halbach array," *IEEE Trans. Magn.* **40**, 2068–2070 (2004).
- ¹⁷M. Cruz-Hernandez, D. Grant, and V. Hayward, "Haptic devices having multiple operational modes including at least one resonant mode," U.S. Patent No. 7,369,115 (2008).
- ¹⁸I. Poupyrev and S. Maruyama, "Tactile interfaces for small touch screens," in *Proceedings of the 13th Annual ACM Symposium on User Interface Software and Technology (UIST '03)* (2003), Vol. **5**, pp. 217–220.
- ¹⁹H.-Y. Yao, V. Hayward, and R. E. Ellis, "A tactile enhancement instrument for minimally invasive surgery," *Comput. Aided Surg.* **10**, 233–239 (2005).
- ²⁰H.-Y. Yao and V. Hayward, "An experiment on length perception with a virtual rolling stone," in *Proceedings of the Eurohaptics* (2006), pp. 325–330.
- ²¹H.-Y. Yao and V. Hayward, "A network-ready multi-lateral high fidelity haptic probe," in *Symposium on Haptic Interfaces for Virtual Environment and Teleoperator Systems* (2006), pp. 81–82.
- ²²W. M. Leach, "Loudspeaker voice-coil inductance losses: circuit models, parameter estimation, and effect on frequency response," *J. Audio Eng. Soc.* **50**, 442–450 (2002).
- ²³C. Alexander and M. Sadiku, *Fundamentals of electric circuits* (McGraw-Hill, New York, 2004), Chaps. 2 and 13.
- ²⁴J. Eargle, *Loudspeaker Handbook* (Springer, Heidelberg, 2003), Chap. 1, pp. 3–14.
- ²⁵J. Miles, "Applications and limitations of mechanical-electrical analogies," *J. Acoust. Soc. Am.* **14**, 183–192 (1943).